Journal of Hydrology: Regional Studies 52 (2024) 101736

Contents lists available at ScienceDirect

Journal of Hydrology: Regional Studies

journal homepage: www.elsevier.com/locate/ejrh

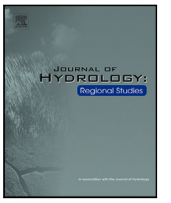

Distinct geographical and seasonal signals in two tree-ring based streamflow reconstructions from Tasmania, southeastern Australia

Kathryn J. Allen [a,b,*], Danielle C. Verdon-Kidd [c], Mandy B. Freund [d], Carly R. Tozer [e], Jonathan G. Palmer [f,g,h], Philippa A. Higgins [f,g,i], Krystyna M. Saunders [j,k], Patrick J. Baker [b]

[a] School of Geography, Planning, and Spatial Sciences, University of Tasmania, Australia
[b] School of Agriculture, Food and Ecosystem Sciences, University of Melbourne, Australia
[c] School of Environmental and Life Sciences, University of Newcastle, Australia
[d] CSIRO Environment, Melbourne, Australia
[e] CSIRO Environment, Hobart, Australia
[f] School of Biological, Earth and Environmental Sciences, University of New South Wales, Sydney, Australia
[g] Australian Research Council Centre of Excellence in Australian Biodiversity and Heritage, University of New South Wales, Sydney, Australia
[h] Chronos 14Carbon-Cycle Facility, Mark Wainwright Analytical Centre, University of New South Wales, Sydney, Australia
[i] Water Research Centre, School of Civil and Environmental Engineering, University of New South Wales, Sydney, Australia
[j] Australian Nuclear Science and Technology Organisation, Lucas Heights, Australia
[k] Institute of Marine and Antarctic Science, University of Tasmania, Australia

ARTICLE INFO

Keywords:
Australia
Tasmania
Streamflow
Subtropical ridge
Seasonal signature
Geographic signature

ABSTRACT

Study region Western Tasmania, southeastern Australia.

Study focus We present two new tree-ring based inflow reconstructions from western Tasmania in southeastern Australia.The warm season reconstruction (Dec–Feb) extends from 1030–2007 CE and explains up to 42% of the variance in instrumental flow, while the cool season (JA) extends from 1550–2007 CE and explains 27% of instrumental flow variance. Key features include an extended pluvial period in the 11th Century and a protracted dry period in ~1500CE, neither of which are represented in the DJF instrumental record. Decreasing JA flow since the 19th Century is consistent with a local sediment-based hydroclimate record.

New hydrological insights for the region The reconstructions confirm that the instrumental data do not capture how protracted past low or high flow periods have been. It is therefore important to consider pre-instrumental flow data when planning for the future. The reconstructions provide new insights into regional variability through their association with the Subtropical Ridge (STR) and the Southern Annular Mode (SAM). Differing spatial signatures of the seasonal reconstructions, and their associations with season-specific impacts of STR and SAM, highlight the need for caution when considering the use of remote hydroclimate proxy records with strong seasonal signatures. The reconstructions suggest that extrapolation of seasonally defined reconstructions to represent annual flow for regions beyond the extent of their spatial footprint may be problematic.

* Corresponding author at: School of Geography, Planning, and Spatial Sciences, University of Tasmania, Australia.
E-mail address: Kathryn.Allen@utas.edu.au (K.J. Allen).

https://doi.org/10.1016/j.ejrh.2024.101736
Received 14 August 2023; Received in revised form 22 February 2024; Accepted 10 March 2024
Available online 19 March 2024

1. Introduction

It is unequivocal that human actions have contributed to globally increasing temperatures, and there is high confidence that the observed increase in hot extremes across almost all the world's regions is associated with anthropogenically induced change (Masson-Delmotte et al., 2021). There is less certainty, however, around the role that human-induced change has had on global hydroclimate and its extremes, and how these are likely to evolve in the future (Masson-Delmotte et al., 2021). Short instrumental records of only ~50–100 years impede our ability to assess long-term hydroclimate variability (Consortium et al., 2017). Without adequate understanding of the extent of natural variability, it is difficult to appreciate the impact of contemporary climate change on hydroclimate, or to improve our confidence in hydroclimate projections.

In Australia, recent severe drought and flood events are a reminder that Australia has one of the most variable hydroclimates in the world (Peel et al., 2004). While the Millennium Drought that afflicted southeastern Australia (nominally 2001–2009) appeared exceptional in instrumental records (2001–2009; Van Dijk et al., 2013), it is unlikely that the short time-series of instrumental data are able to capture just how extreme or prolonged droughts or pluvial periods in Australia can be (e.g. Verdon-Kidd and Kiem, 2010; Ho et al., 2015; Allen et al., 2015; Vance et al., 2015, 2022; Freund et al., 2017; Verdon-Kidd et al., 2017). Various palaeo-records have demonstrated that Australia has experienced more extreme floods (Allen et al., 2020b and references therein) and droughts (Cook et al., 2022 and references therein) in the past. Australian water authorities are well aware of the issues associated with relying on short records for planning future investment and have supported a number of efforts to extend water availability records back in time (Tozer et al., 2016, 2018a; Vance et al., 2022; Kiem et al., 2020; Allen et al., 2015, 2017). Through providing a much longer record, palaeo-proxy records can help inform the adequacy of existing and planned infrastructure (Stockton and Jacoby, 1976; Woodhouse et al., 2010; Cook et al., 2022), urban, agricultural and industrial water-supply planning, and water allocation plans, as well as planning for future production of renewable hydropower resources.

At present there are only a few seasonally to annually resolved hydroclimate reconstructions, or records related to hydroclimate, for various parts of Australia (Lough, 2007, 2011; Lough et al., 2015; Gallant and Gergis, 2011; Heinrich et al., 2008, 2009; Palmer et al., 2015; Verdon-Kidd et al., 2017; Allen et al., 2017; Vance et al., 2022; Tozer et al., 2018a; Allen et al., 2020a; Kiem et al., 2020; O'Donnell et al., 2021). To date, the longest of these come from southwestern Western Australia (O'Donnell et al., 2021) and the central east coast of Australia (Tozer et al., 2016, 2018a; Kiem et al., 2020). Many of these accurately dated annual and seasonal reconstructions, however, rely on remote proxies largely due to the relative lack of suitable proxies on mainland Australia (Gallant and Gergis, 2011; Palmer et al., 2015; Verdon-Kidd et al., 2017; Freund et al., 2017; Verdon-Kidd et al., 2017; Tozer et al., 2018a, 2016; Kiem et al., 2020; O'Donnell et al., 2021; Higgins et al., 2023). This heavy reliance on remote proxies may be problematic if there is a mismatch in the seasonal target and the sensitivity of the remote proxy, or if there are multiple (and potentially interacting) hydroclimate drivers in both the target and proxy source regions. To date, the focus of efforts to reconstruct hydroclimate has been on producing credible and useful reconstructions for specified target regions. However, an increasing emphasis on better understanding past temporal and spatial hydroclimate variability means it is necessary to pay more attention to the context and limitations, as well as the strengths, of hydroclimate reconstructions. This is directly relevant to advancing the fourth phase of the Past Global Changes (PAGES) 2k initiative focusing on hydroclimate (https://pastglobalchanges.org/publications/pages-magazines/pages-magazine/129037).

In this study, we present two new dam inflow reconstructions for western Tasmania in southeastern Australia based on tree-ring records that are local to the region. One reconstruction is for the summer months (December–February; DJF; warm season) and the other is for the winter months (July–August; JA; cool season). The key reason we focus on reconstructions of specific seasons relates to the differing demands placed on water resources for electricity generation in these two different seasons. Additionally, the broadscale drivers of precipitation over the region vary in their strength and impact in different seasons. Using these two reconstructions, we assess how well the instrumental data capture extremes in the longer record. We also investigate how these reconstructions relate to the broader southeastern Australian hydroclimate. We ask: is it possible to derive information about past hydroclimate over the broader Australian region from these particular reconstructions and, in particular, does seasonality matter?

2. Materials and methods

The Australian island state of Tasmania lies between 40 and 44°S and 144 and 149°E within a prevailing westerly airstream. Although geographically small, hydroclimatic conditions on the western and eastern sides of the island differ substantially. Parts of western Tasmania receive up to 3500 mm/yr while in the east, which is subject to a rain-shadow effect, annual rainfall is generally between 500 and 700 mm. Average annual rainfall across the study area is approximately 1500 mm/yr (Fig. 1). Tasmania's weather and climate is affected by multiple broad- and synoptic-scale processes including the El Niño-Southern Oscillation (ENSO) and its related low frequency expression in the Interdecadal Pacific Oscillation (IPO), the Indian Ocean Dipole (IOD), the Southern Annular Mode (SAM), Pacific South American pattern (PSA), and atmospheric blocking (Hill et al., 2009; Risbey et al., 2009; Tozer et al., 2018b; Ma et al., 2022). Seasonal movement of the sub-tropical ridge (STR) and the observed southward expansion of the Hadley Cell over Australia also have important impacts on the state's climate (Post et al., 2014; Nguyen et al., 2015).

2.1. Catchment data

We use the augmented catchment inflow records for three lakes (Lakes Burbury, Gordon and Murchison) in western Tasmania (Fig. 1A) as our reconstruction targets. These catchments are located in the high rainfall west Tasmanian region where the major

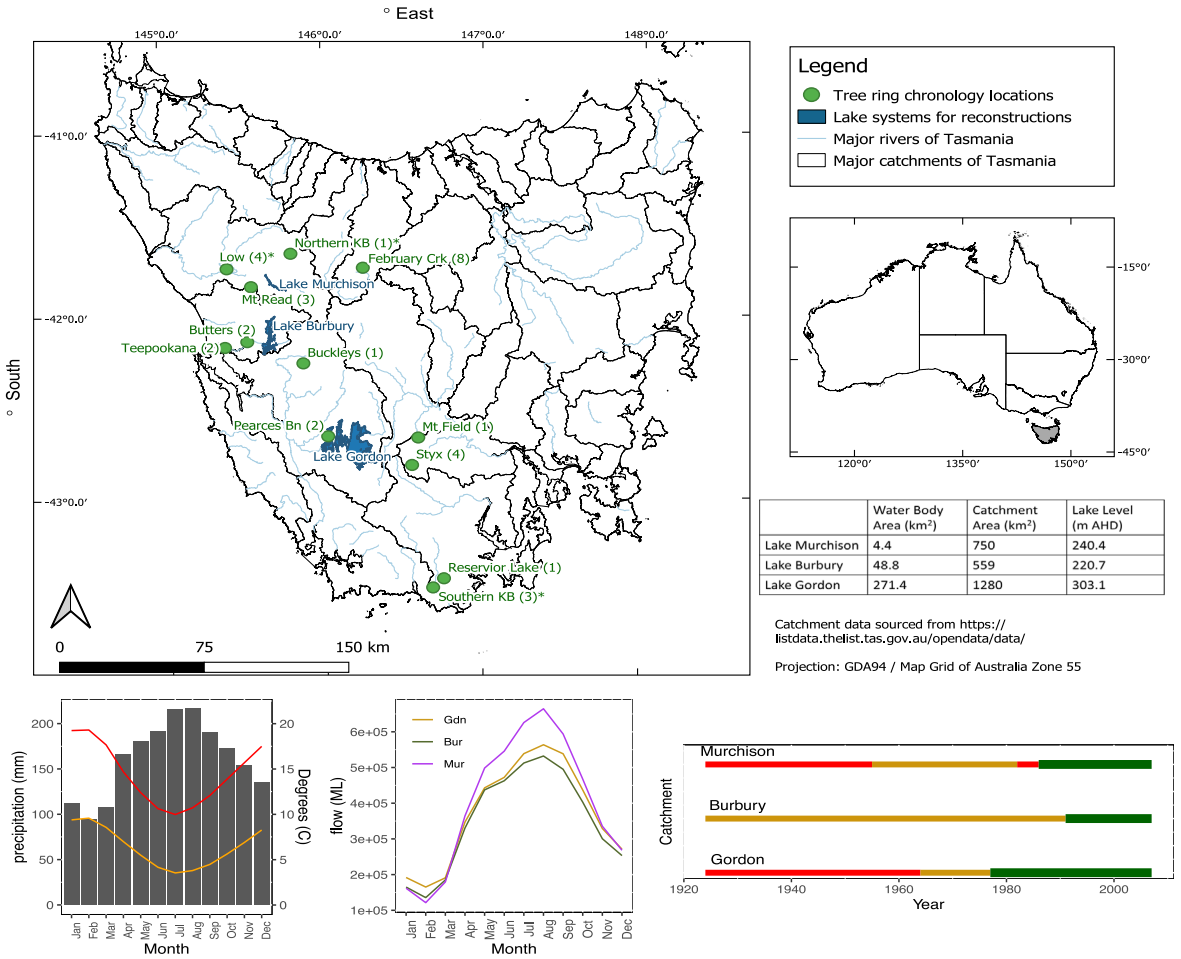

	Water Body Area (km²)	Catchment Area (km²)	Lake Level (m AHD)
Lake Murchison	4.4	750	240.4
Lake Burbury	48.8	559	220.7
Lake Gordon	271.4	1280	303.1

Fig. 1. A. Location of individual tree ring chronologies used to reconstruct inflows. The location of the three lake systems for which inflows were the reconstruction target are also shown. Numbers next to the tree-ring sites indicate the number of chronologies for that site. B & C. Climatology of the study region. In B, bars represent monthly precipitation, red line is maximum temperature and orange line is minimum temperature. In C, the flows are shown for the individual catchments used to represent the region (see Fig. 1A for locations). Temperature and precipitation for the study area are drawn from the CRU4.07 data, downloaded from KNMI Climate Explorer (https://climexp.knmi.nl/). The inflow data is that used in this study. D. Methods of estimating/measuring inflow to catchments over time. Red — regression type estimates; yellow, measured flow into catchment; green current modelling approach of catchment inflow. (For interpretation of the references to colour in this figure legend, the reader is referred to the web version of this article.)

storages used to produce approximately 60% of Australia's hydropower are located. Flow into these catchments has not been directly measured for the entirety of the respective records, with periods in most records modelled using different methodologies through time (Fig. 1B). The most reliable parts of these records are direct measurements and associated modelling that extend from the present back to the early 1970s, followed by measurements of flow into catchments but without use of current modelling approaches. The earliest parts of the available data series rely on regressions with poor quality data from a single gauge in western Tasmania. We therefore restricted our use of these records to the post-1940 period. Summer inflow accounts for approximately 13% of water year (Jul-Jun) inflows (Gordon 13%; Burbury 14%; Murchison 13%); while Jul-Aug flows account for approximately 27% of water year inflow (Gordon 25%; Burbury 25%; Murchison 27%). Strong interrelationships amongst catchment flows (Table S1) for both seasons are consistent with catchment locations and methods used to estimate flow prior to availability of direct inflow measurements and modelling practices (Fig. 1).

2.2. Tree-ring data

The tree-ring reconstructions are based on a range of previously developed tree-ring series described in the references listed below. These series have been developed from four endemic Tasmanian tree species (*Lagarostrobos franklinii, Athrotaxis selaginodies, Athrotaxis cupressoides* and *Phyllocladus aspleniifolius*) and are a mixture of ring width and wood properties (density, tracheid radial diameter, cell wall thickness, microfibril angle) data. Each of these different chronology types encodes a slightly different climate

signal (e.g., by season) or records a different response to the same variable (e.g., sign of the relationship). Consequently, there are multiple chronologies for some sites (Fig. 1A). Details concerning the development of these individual chronologies can be found in Drew et al. (2013) and Allen et al. (2015, 2017, 2018, 2022). The chronologies selected through the process described below are shown in Table S2 and the number of samples and chronologies are shown in Figure S1. It is important to note that the relationships exploited in this study do not mimic those that have been commonly identified at a range of sites at their altitudinal and/or latitudinal limits in the Northern Hemisphere (Allen et al., 2018, 2022; Björklund et al., 2023; Wilson et al., 2021; Schneider et al., 2015). While the reasons for this are not entirely clear, two important factors stand out. Firstly, the Northern Hemisphere species examined are typically strongly temperature-limited due to their location at high latitude and/or high altitude (>1000 m ASL) sites. In contrast, Tasmania experiences a temperate maritime climate (Grose et al., 2010) in which seasonal temperature and hydroclimate extremes such as those affecting regions like the European Alps or Fennoscandia (temperature), or southwestern United States or central Australia (hydroclimate), do not occur. The second factor concerns the species physiology. *L. franklinii* is highly moisture sensitive with limited stomatal control, making it highly susceptible to drought (Brodribb and Cochard, 2009). This sensitivity is consistent with the positive relationship between the wood properties of this species and flows (Table S2; Allen et al., 2022). The situation is more complex for both *P. aspleniifolius* and the *Athrotaxis* spp. The latter typically displays a negative relationship between tracheid radial diameter and flow and a positive relationship between both density and cell wall thickness and flow while the former species exhibits the opposite response (Table S2, Allen et al., 2022). The difference in relationships between climate and anatomical properties across species and sites is not unique to the Tasmanian species, with a range of previous work also noting variation in climate relationships that appear related to both site and species characteristics (Martin-Benito et al., 2013; Blake et al., 2020; Rocha et al., 2020; Wilson et al., 2021). Understanding the complex relationships between climate and anatomical wood properties remains an active area of research.

Ring-width series were standardised with an age-dependent smoothing spline (Melvin et al., 2007) for sites where there was evidence of an age-related growth trend in a sufficient number of individuals. This spline is more flexible in the early years but becomes increasingly stiff in the later years of growth, and hence less responsive to local variability in latter years of growth. A stiff Friedman supersmoother (Friedman, 1984) was used to standardise (remove non-climatic related variance) in series in the remaining chronologies, including wood properties chronologies, which did not generally exhibit age-related trends. All chronologies were produced using a signal-free detrending methodology to better preserve medium-frequency variation (Melvin and Briffa, 2008). All selected chronologies are from sites located in western Tasmania (Fig. 1).

2.3. The reconstructions

Previous work reconstructed west Tasmanian streamflow for early summer (December–January) and mid-winter (July–August; JA) (Allen et al., 2015, 2017). The availability of some additional site chronologies (e.g., density, tracheid radial diameter and cell wall thickness for a number of *L. franklinii* sites has made it possible to extend the warm season reconstruction window to also include February (DJF). However, it was neither possible to produce a reconstruction that was successfully validated for an extended (JJA or longer) cool season nor for the water-year (July–June) flow. This was most likely due to the strong seasonal dependence of the many of the tree-ring predictors, particularly the wood properties chronologies (Allen et al., 2022).

Prior to developing the two seasonal (DJF and JA) reconstructions, we checked that it was possible to develop validated reconstructions at the individual catchment level (data not shown, but each developed in the same manner as the reconstructions shown here). See locations of these catchments in Fig. 1. This also allowed us to confirm that the relationships amongst these reconstructions were comparable with those amongst the instrumental flow series (Table S1). Validating reconstructions for individual catchments, and correlations amongst catchments, that were similar to the instrumental data supported the development of regional reconstructions. To account for substantially different catchment sizes (Fig. 1), total seasonal flows (DJF and JA) for each catchment were converted to z-scores before being averaged to produce a regional target flow series for each season.

To identify potential predictor chronologies, we examined the association between potential pre-whitened predictors and target inflow series using two-tailed tests across three different measures of correlation (Pearson's R, Spearman's R and the robust Pearson's R). Only predictors significant at $p < 0.1$ were passed to the principal components stage of modelling (Table S2). In addition, we used only that portion of chronologies that contained at least n = 5 samples. Each reconstruction utilised a nested principal component regression approach, common in a large body of previous work (e.g., Cook et al., 1999, 2013; Seftigen et al., 2017). Each of the nested reconstructions was rescaled using the mean and standard deviation of the instrumental data to capture lost variance due to regression in the calibration period and to avoid artificial variability associated with differences in R^2. The successively longer reconstructions were then spliced together to produce the final reconstruction. A measure of uncertainty around the estimates was obtained through bootstrapping both the predictors and inflow series (300 replications; Vinod and López-de Lacalle, 2009). This process also enabled the non-parametric estimation of calibration and validation statistics which are described below. We used the most recent period,1963–2007, for which data quality was generally higher, to calibrate our models, leaving 1940–62 for model validation. Use of this longer calibration period (rather than a more traditional split of 50%-calibration and 50% validation) also aimed to minimise the possibility of the no-analogue issue that may arise if the full range of flow values is not captured in the calibration period. Although inflow data extend beyond 2007, several of the tree-ring chronologies in the potential predictor pool do not. The earliest dates of the reconstructions were dictated largely by the availability of predictors meeting the selection criteria, but also by the period over which the Reduction of Error (VRE) interval estimates remained above zero and the Coefficient of Efficiency (VCE) point estimates were greater than zero.

Model calibration statistics include R^2 (CRSQ) and the cross-validation reduction of error statistic (CVRE) calculated using a leave-one-out procedure. The CVRE statistic can provide a less biased estimate of model fit than CRSQ. Model validation statistics included R^2 (VRSQ), VRE and VCE, Cook et al. (1999) . VRE and VCE values >0 indicate that the model is superior to climatology for the validation period. Whereas VRE uses the mean of the calibration period in its calculation, VCE uses the mean in the validation period, making it more difficult to achieve a value >0 (and is therefore a stricter threshold). Note that the formulation of the VRE statistic is similar to the Nash–Sutcliffe Efficiency (NSE) statistic more commonly used in hydrology. The key difference is that VRE is based on comparing the sum of the squared differences of the instrumental and reconstructed data for the verification period with the sum of the squared differences of the verification period data and the mean of the calibration period. In comparison, NSE compares the sum of the squared differences of the instrumental data and reconstructed data divided by the sum of the squared differences of the reconstructed data and the mean of the instrumental data.

2.4. Comparison with regional hydroclimate data, climate indices and volcanic eruptions

We compared the post-1940 portion of our reconstructions with other available hydroclimate data and large-scale climatic processes. First, we examined how the reconstructed series and both precipitation and flow across southeastern Australia were related across their entire common period. The primary reason for doing this is to address the question of whether or not our reconstructions might provide useful long-term information about hydroclimate beyond western Tasmania since there are currently very few palaeo-hydroclimate records for continental Australia. We used precipitation data from the Australian Gridded Climate Dataset (AGCD; Jones et al., 2009) and a selection of streamflow stations in the Bureau of Meteorology Hydrologic Reference Station network (http://www.bom.gov.au/water/hrs/) from southeastern Australia. For streamflow, we aimed for representation across multiple catchment basins in the region. We limited the comparison to those stations with a >40-year overlap with the reconstructions. Using both precipitation and streamflow data allowed us to better consider the robustness of the results. We also compared the entire reconstructions series with the indices outlined below.

Second, we considered how extremes in both the post-1940 instrumental data and the reconstructions were associated with broadscale processes, and whether these relationships appeared to differ from those for the entire time series. We created composites of the 10 wettest and 10 driest years in both the reconstructions and instrumental data for the 1940–2007 period in both data sets. These composites were created for the DJF and JA seasons of the reconstructions as well as the climate data. No lagged relationships were tested. We compared mean 850 geopotential height (GPH) for each of these composites with the mean of the remaining data (two-sided *t*-test) to identify large-scale atmospheric pressure patterns associated with extremes. We also examined relationships between the 10-year composites and a range of indices (all data detrended) representing processes such as the El Niño-Southern Oscillation (ENSO; http://www.bom.gov.au/climate/enso/nino34-monthly.txt), the Southern Oscillation Index (SOI; http://www.bom.gov.au/climate/enso/soi_monthly.txt), the Southern Annular Mode (SAM; https://legacy.bas.ac.uk/met/gjma/sam.html), the Indian Ocean Dipole (IOD; https://psl.noaa.gov/gcos_wgsp/Timeseries/DMI/), the Subtropical Ridge (STR; Drosdowsky, 2005; Larsen and Nicholls, 2009), and atmospheric blocking (McBride and Nicholls, 1983; Power et al., 1999; Drosdowsky, 2005; Pezza et al., 2008; Risbey et al., 2009; Murphy and Timbal, 2008; Pook et al., 2013; Hendon et al., 2014). We included blocking indices for 5° intervals because the location of impacts will depend on the longitudinal position of atmospheric blocking (data kindly provided by M. Pook, CSIRO). In addition, we used multiple indices (e.g., Blocking, SAM, ENSO) for some processes to check for consistency of relationships across the indices. Other processes that operate at interdecadal scales, such as the Interdecadal Pacific Oscillation (IPO; Power et al., 1999), were not considered here because longer data sets are required to assess them, particularly for indices that exhibit significant serial persistence (King et al., 2014).

Third, we compared our reconstructions with four other annually resolved streamflow reconstructions available for continental southeastern Australia. These comparisons were made for the full period of overlap between the paired series. Each of these relies on remote proxy data due to the lack of *in situ* palaeoclimate records in this region. The Williams River (Tozer et al., 2018a), and two of the three Murray River reconstructions (Ho et al., 2015; Gallant and Gergis, 2011) are independent of the new Tasmanian reconstructions, but the more recent Murray River construction (Higgins et al., 2023) uses one of the same chronologies as the DJF reconstruction here (TNE_TRD; Table S2). As a point of interest, we also included a lake-based precipitation reconstruction from northwestern Tasmania, primarily because it is the only other relatively high-resolution (nominally ~5-yearly) precipitation or streamflow reconstruction local to Tasmania that is completely independent of our new reconstructions.

Lastly, a volcanic influence on JA inflow in western Tasmania has tentatively been identified (Allen et al., 2017). As the new JA reconstruction is almost 200 years longer than the original, and the DJF reconstruction is close to 1000 years in length, we compared the reconstructions with two volcanic indices (for the same seasons) that model the aerosol loading for different latitudes (Toohey and Sigl, 2017; Gao et al., 2008). We extracted values for the Tasmanian latitudes (i.e. 40 to 45°S). Aerosol values that were at least 2σ greater than average were used to identify relevant volcanic eruptions used in a superposed epoch analysis (SEA; using *dplR* in R; Bunn, 2008). In cases where an identified eruption occurred within 10 years of a candidate eruption for the SEA, data in the reconstruction were removed and values from the next non-volcanically active period inserted instead.

3. Results and discussion

3.1. The December–February reconstruction

The regional warm season inflow reconstruction (1020–2007 CE) is strongly correlated with the instrumental data for their overlapping period (1940–2007; Fig. 2). Explanatory power over the calibration period (CRSQ = 0.415; Fig. 2) is typical of many

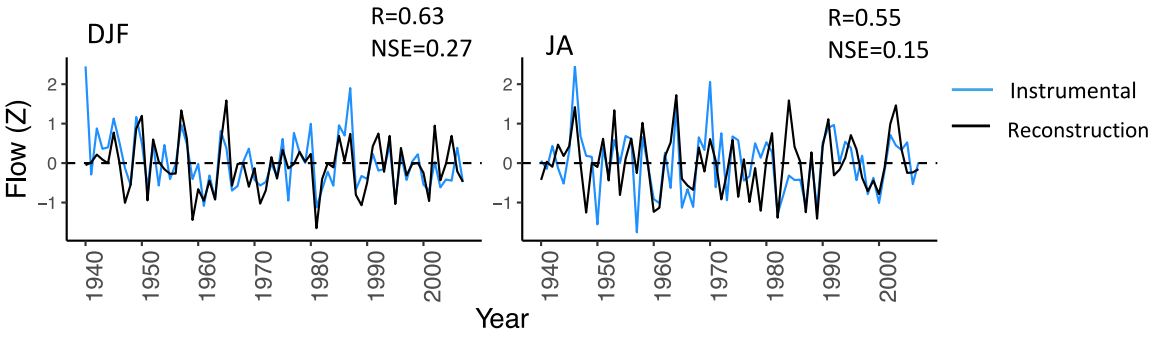

Fig. 2. Instrumental record and the regional reconstructions for the two seasons. Note that flows have been converted to z-scores. The NSE statistic is the Nash–Sutcliffe Efficiency commonly used in hydrology and has been estimated over the period of overlap between the instrumental period data and the reconstructions.

flow reconstructions elsewhere in temperate climates and mesic forests (Ljungqvist et al., 2020). As expected, explanatory power decreases back in time as the number of predictors declines, dropping to approximately 26% in the earliest reconstruction nest. Nevertheless, both the point and interval estimates of the strictest verification statistic, VCE, remain positive for the entire length of the reconstruction.

The inflow reconstruction indicates a protracted and intense pluvial period at the start of the record that is much wetter than any period during the instrumental record. The protracted low-flow period that extends from the late 15th Century into the first quarter of the 16th Century (Fig. 3) is also longer and more severe than any dry period occurring in the instrumental record. The driest individual year was 1512 CE and the driest decades were 1300–09 and 1660–69 CE. Maximum drought length simulations (based on annual data) across Australia also indicate longer droughts occurred in the pre- than post-instrumental era (Falster et al., 2023). Documentary evidence (Evans, 2012) for drought during much of 1908, is consistent with it being identified as one of the top 10 dry events in the reconstruction (Table S3). The wettest year was 1093 and the wettest decade was 1090–1099 CE (Fig. 3, Table S3).

The overall distribution of instrumental inflows (1940–2007) shows that relatively dry conditions have been more common after 1940 than before (Fig. 3), which also agrees with Falster et al. (2023). A fatter upper tail of the instrumental data distribution also suggests that very wet extremes have also been more common since 1940. The pre-instrumental warm season distributions are slightly more leptokurtic than those for the instrumental data, suggesting greater clustering of events around the mean (Fig. 3). However, it is apparent that protracted downturns like those in the late 13th and 15th–16th Centuries are not represented in the instrumental period (Fig. 3).

3.2. The July–August reconstruction

The correlation between the JA inflow reconstruction and instrumental data for the entire 1940–2007 period is 0.551 (Fig. 2). Overall, the calibration and validation statistics for the shorter JA reconstruction (1550–2007 CE) are weaker than for the DJF reconstruction (Fig. 3, CRSQ = 27% in the most recent nest and 16% in the earliest nest). However, both VRE and VCE remain above zero (Fig. 3), indicating that the reconstruction provides meaningful insight into past hydroclimate in western Tasmania. Higher explained variance for the validation than calibration period may be associated with a relatively short verification period.

The downward trend in the cool season flow since the early 19th Century is unusual in the longer-term context of the reconstruction (Fig. 3). Superimposed on this decline is a late 20th Century trend towards slightly wetter conditions. Simulations also indicate that drought frequency and time in drought per century across Tasmania have increased in the 20th Century relative to the previous 1000 years (Falster et al., 2023). The lowest reconstructed flow occurred in 1909 (Table S3, Fig. 3) and the driest decades were 1970–79 and 1910–19 CE (Table S3). Drought occurred across the state from September–December of 1909, but floods were recorded for June and August in the south and west (Evans, 2012). The year 1919 (also one of the 10 driest years; Table S3) experienced drought from August–December (Evans, 2012). Three of the driest decades occurred in the latter part of the 20th Century (1960–89) with three intense dry periods from the late 19th to early 20th Century (Fig. 3, Table S3). The highest reconstructed flow was in 1816, which is consistent with the occurrence of floods in July and August across Tasmania (Evans, 2012) that year. The wettest reconstructed decades were 1810–19 and 1560–69 CE (Table S3). Documentary records exist for three other wet years in the top 10 (1832, 1908, 1928). Winter floods and/or heavy snow were recorded for two of these (1832 and 1928) (Evans, 2012).

While the distribution of cool season inflow values for the recent period does not appear exceptional in the longer context (Fig. 3), dry events have been more likely after than before 1940 and extreme wet events have become less common after than before 1940. It is worth noting, however, that the cool season reconstruction does not extend back to the protracted dry period from 15th-early 16th Century observed in the DJF reconstruction.

Even more concerning than the decline in wet events for JA (Fig. 3) is the persistent trend towards an increasing drought deficit since the late 19th Century (Fig. 4). This deficit was determined by summing the z-scores of consecutive years for which flows for

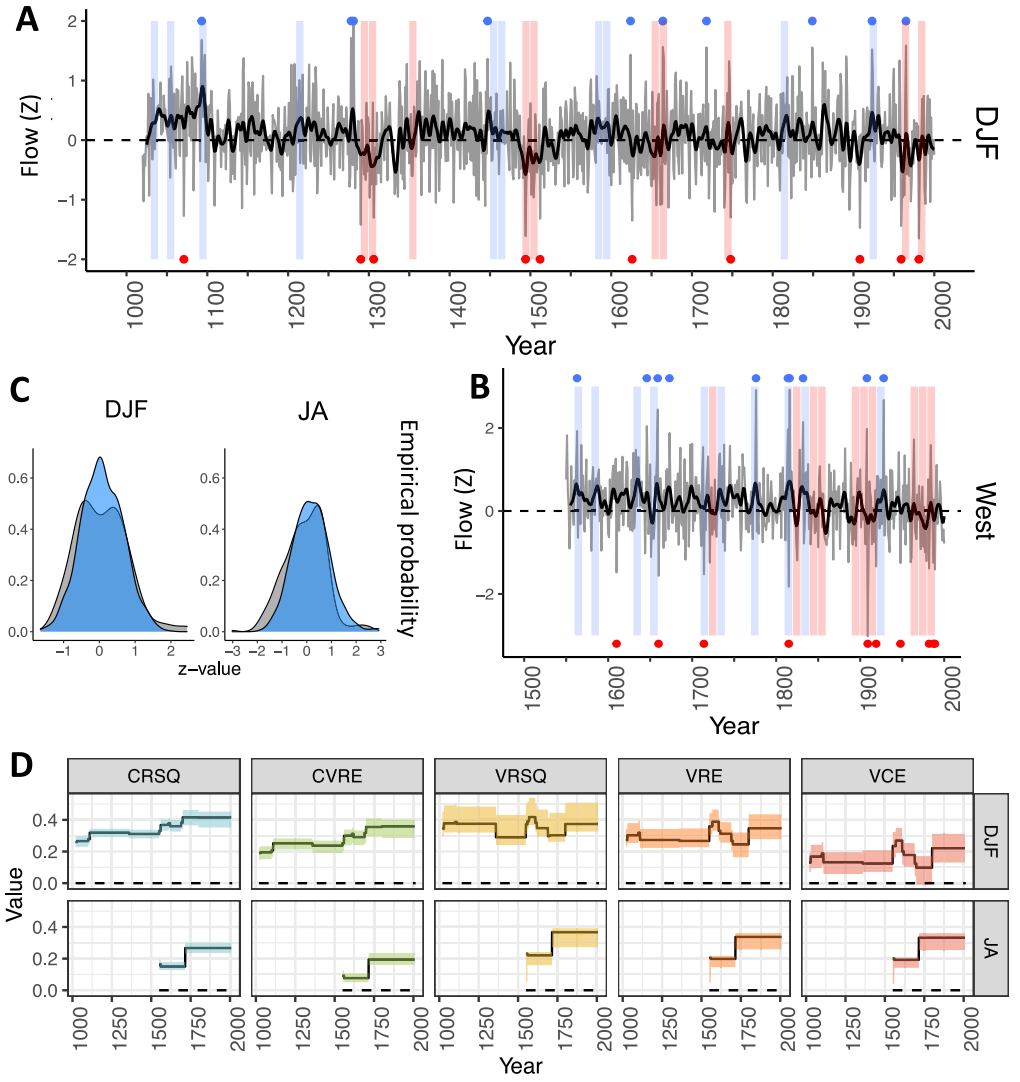

Fig. 3. Regional reconstructions, extremes and characteristics. Thick black line in A & B is 20-year Gaussian smoothed flow. Blue and red dots identify the 10 wettest and driest individual years respectively and blue and red bars identify the 10 wettest and driest 10-year periods respectively. See Table S2 for years and decades C. Probability distributions for instrumental period (grey) and reconstructed flows (blue). D. Reconstruction statistics for all reconstruction nests. Ribbon is the 90% bootstrapped interval for each statistic. Top: DJF reconstruction, bottom, JA reconstruction. (For interpretation of the references to colour in this figure legend, the reader is referred to the web version of this article.)

both seasons were lower than the average of the 1940–2007 period. Drought deficits were also common in the mid-17th Century. Continued flow deficits without regular recharge have significant implications for the ability to generate hydroelectricity in Tasmania and will become an increasing concern for water managers. Enhanced variability in deficit/surplus, such as observed in the 17th to mid-18th Century, increases uncertainty in forecasting supply and also has important implications for managing and regulating water storage levels into the future.

3.3. Relationships with large-scale processes

There are clear seasonal differences in the relationships between west Tasmanian hydroclimate (reconstructions and instrumental data) and hydroclimate records across southeastern Australia (Fig. 5). For JA, there are strong positive relationships between the flows into western catchments and those across Tasmania as well as the southernmost part of mainland Australia. The negative relationship between the west Tasmanian inflows and the central east Australian coast for the instrumental flow data is not well captured in the reconstruction, however, and the modest strength of the reconstructions likely plays a role here. In DJF, a positive relationship between west Tasmanian flow (both instrumental and reconstructed) becomes limited to western Tasmania, but the negative correlation with coastal eastern Australia is more consistent between the reconstructions and instrumental data.

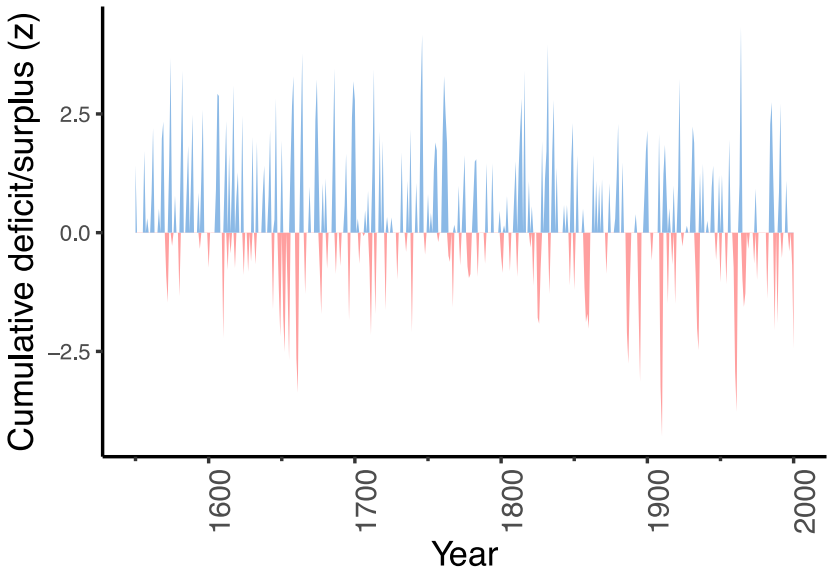

Fig. 4. Cumulative deficits and surpluses for those years in which both seasons experience a deficit (surplus). Red represents deficits, blue surpluses. Values only shown for years in which inflows were less (more) than the mean of the 1940–2007 instrumental data period. (For interpretation of the references to colour in this figure legend, the reader is referred to the web version of this article.)

Relationships between west Tasmanian inflow (instrumental and reconstructed) with broadscale processes are clearest for STR_L (latitude of the STR; positive), STR_I (Intensity of the STR; negative), and SAM (negative; Table 1). This is the case for both seasons. Significant relationships with atmospheric blocking, especially when located further east occur for the instrumental JA data, but not the reconstructed flow. These same processes are relevant to the broader southeast Australian region, as is ENSO (Table 2, Williams and Stone, 2009; Drosdowsky, 2005; Murphy and Timbal, 2008; Timbal and Drosdowsky, 2013; King et al., 2014). The results for the STR are not surprising. Well known as a leading source of cool season rainfall variability, the STR accounts for 30%–50% of rainfall variability in coastal south Queensland and Tasmania (Pittock 1971 in Williams and Stone, 2009). Its seasonal movement of up to 12° between August and February (Figure S2) has also been shown to produce seasonally distinct geographical impacts on hydroclimate (Drosdowsky, 2005; Murphy and Timbal, 2008; Timbal and Drosdowsky, 2013) that are consistent with the results obtained for Tasmania, and further north (Table 1, Fig. 5). For example, a more northerly STR and storm belt accompanied by low pressure anomalies in the cool season is consistent with higher precipitation and streamflow over southern Australia. This is reflected in the positive relationships ($p < 0.05$) between the JA reconstruction and flow and precipitation across the Australian far southeast (Fig. 5). It is also associated with a negative relationship between Tasmanian hydroclimate ($p < 0.05$) and that further north for JA (Fig. 5, Table 2).

The opposite sign in SAM-precipitation relationships for both seasons for the central east Australian coast and western Tasmania is well known (Fogt and Marshall, 2020) and is again consistent with the data in this study (Fig. 5, Table 2).

The spatial patterns of GPH850 anomalies related to wet and dry extremes since 1940 also indicate the importance of regional scale drivers of local hydroclimate (Fig. 6 & Figure S3). Particularly wet events in both seasons are associated with low pressure anomalies across southeastern Australia and hemispheric regions of anomalously high GPH extending south from approximately 55°S. In the warm season, these high pressure anomalies are reduced to an area to the immediate north of the Ross Sea. Dry events are related to high pressure anomalies to the south of the Australian mainland and occur at lower latitudes in the summer months (Fig. 6, Figure S3).

The regional-scale drivers (STR_L, STR_I, SAM) most strongly related to the 1940–2007 Tasmanian flow reconstructions and instrumental data are also associated with wet and dry event composites (Table 1). There is, however, some asymmetry in their influence on extremes, and this is consistent with stronger GPH anomalies for wet compared to dry extremes (Fig. 6) In JA, a lower latitude and more intense STR, and negative SAM, are strongly associated with wet events, whereas their relationship with dry events is weaker, especially in the instrumental data (Fig. 7). For DJF, STR_I has a more symmetrical association with wet and dry events, but STR_L becomes less important for either wet or dry events (Fig. 7). High DJF flow events are associated with negative SAM anomalies but the reverse is not true for dry events (Fig. 7).

Both our seasonal inflow reconstructions also have some important similarities with an approximately 5-year resolution lake sediment record from Rebecca Lagoon in northwestern Tasmania that has been linked to variability in the Southern Hemisphere westerly winds (Saunders et al., 2012) and by implication, the STR (Fig. 8). These similarities are most pronounced at the modern end of the record where cumulative dating uncertainty that occurs as depth increases in the lake record is smaller. Both sets of records indicate an overall declining trend since the early 19th Century and also suggest that the 20th Century has been relatively (but not exceptionally) dry compared to the past 500 years. The long-term decline observed in both sets of records Figs. 3; 8 is consistent with

Table 1
Significant correlations between the reconstructions and instrumental data and a variety of indices of large-synoptic scale atmospheric processes over the period in common for the instrumental and reconstructed flow and the respective indices. All indices represent processes known to affect Tasmanian hydroclimate. Blocking indices at 5° intervals (BI140–BI165) were used because the hydroclimate impacts of blocking will depend on the longitude at which it occurs. Orange colours reflect negative correlations and purple, positive. Darker colours indicate significance at $p < 0.01$ and lighter colours indicate significance at $p < 0.05$. The Drosdowsky record ($Dros_L$, $Dros_I$) is based on 150°E while the Larsen record ($Lars_L$, $Lars_I$) is centred on 145°E. Correlations between the blocking indices and the reconstructed and instrumental series cover the 1948–2007 period; the Viterbi index correlations cover 1958–2007, and all other index correlations extend over 1940–2007. See Table S4 for further details, including relationships between the reconstructions and those indices that extend further back in time.

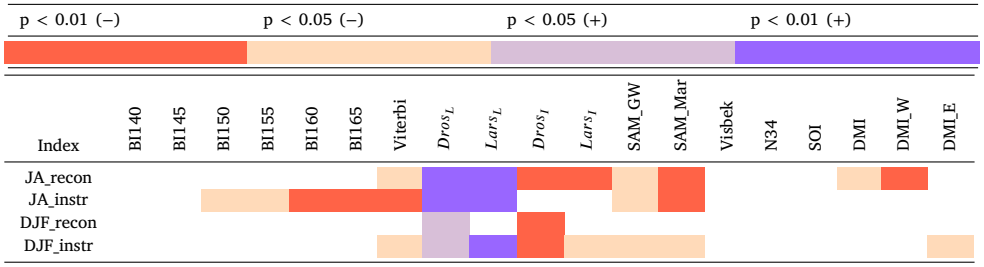

an intensifying STR (Timbal and Drosdowsky, 2013) since at least 1900 and an expanding Hadley Cell, both linked with autumn and winter rainfall declines (Cai et al., 2012; Chiew et al., 2014). Interestingly, another recent low-resolution record based on a bivalve oxygen isotope record from the south Australian coast (Chamberlayne et al., 2023) also indicates drying conditions since around the late 18th Century. In addition, the northwestern Tasmanian sediment record indicates a protracted dry period during the 15th Century, while our warm season flow record suggests a sharp downturn around the end of the 15th Century and beginning of the 16th Century. According to the lake record, the mid-18th Century was relatively dry. Our reconstructions point to dry warm seasons in the first part of the 18th Century and dry winters late in that century. Given increasing dating uncertainty of the sediment record further back in time, it is, however, difficult to assess just how well the records align several centuries ago.

Based on these observations, it is plausible that previous wet periods (Tables 1, 2, Figs. 6, 7) such as that in the 11th Century (warm season) may be associated with a frequently negative SAM index over that period. A recent SAM reconstruction based on data assimilation techniques supports this interpretation, indicating that the SAM was quite negative in the 11th Century (King et al., 2023). Some other SAM reconstructions, do not agree, however, with multiple mismatches with reconstructed hydroclimatic conditions in western Tasmania (e.g., Dätwyler et al., 2018). Conversely, our results suggest it is more difficult to attribute past dry events to positive SAM anomalies (Fig. 7). This observation may be relevant to conflicting interpretations of the state of SAM around 1300CE based on hydroclimate records from southern Australia and charcoal and pollen records from Tasmania (Chamberlayne et al., 2023; Fletcher et al., 2018). In this respect, it may be worth considering the possible relevance of changes in the STR during that period.

Despite evidence for the primary influence of the STR and SAM on west Tasmanian hydroclimate, it is also important to note that relationships between streamflow and the STR likely reflect known relationships between the STR and other processes such as SAM, ENSO and the IOD (Cai et al., 2011; Williams and Stone, 2009; Hendon et al., 2014; King et al., 2014; Maher and Sherwood, 2014; Holgate et al., 2022). These processes are themselves interrelated and relationships amongst them are unlikely to be stable over long periods (Dätwyler et al., 2018; Fogt and Marshall, 2020; Nicholls et al., 1996; Power et al., 1999; Timbal and Drosdowsky, 2013, and references therein). Unstable and/or asymmetric relationships between hydroclimate and SAM (Fig. 7) or the IPO (Power et al., 1999; Tozer et al., 2018a) will also create significant challenges for interpreting drivers of past change.

Finally, identification of external forcing in high-resolution palaeo-reconstructions, such as those based on tree-rings, has largely been limited to temperature reconstructions. This emphasis has partly been driven by strong interest in the short-term impacts volcanic eruptions can have on incoming solar radiation and our ability to represent this in global climate models (Cole-Dai, 2010). Some studies have also concluded that there is limited evidence of a volcanic imprint in the Southern Hemisphere tree-ring archive (e.g., Büntgen et al., 2022), although evidence from New Zealand trees does not support this interpretation (Higgins et al., 2022). Based on the longer JA reconstruction available for analysis in this study, our results support the earlier finding of a potential volcanic signal in cool (Allen et al., 2017), but not warm season, hydroclimate in western Tasmania (Fig. 9). The lack of a similar signal in the DJF reconstruction likely reflects seasonally distinct atmospheric circulation patterns, although investigation of this is well beyond the scope of this study. The impacts are equally strong one and five years after the eruption, but the reason why they are not observed in the intervening years is unclear. This finding is interesting both in terms of signal presence in hydroclimate, and its occurrence in the cool rather than warm season. Together with the work by Higgins et al. (2022), it suggests that a careful reassessment of the presence of a volcanic signal in Southern Hemisphere tree-ring records, as well as the hydroclimate and temperature reconstructions based on them, may be overdue. Recent work on the role of Northern Hemisphere extratropical eruptions also emphasises the need for such a reassessment (Burke et al., 2023).

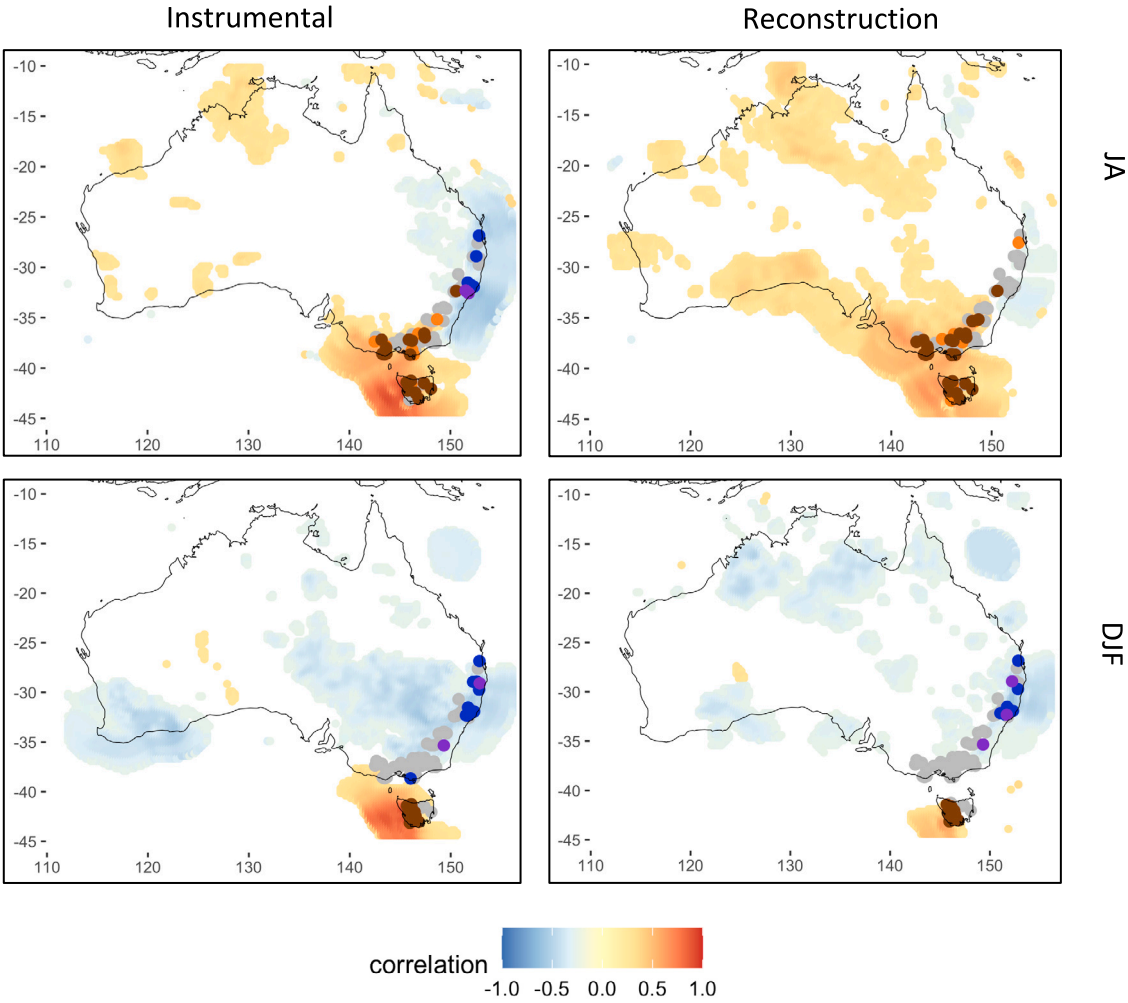

Fig. 5. Correlations between the instrumental data (left) and the new regional streamflow reconstructions (right) and Australia-wide precipitation (shading) and selected hydrological reference stations (data available at http://www.bom.gov.au/water/hrs/). Correlations with precipitation calculated for the period 1940–2007 that is covered by the instrumental data used in this study. Periods used for correlations with streamflow data varied, depending on availability. Grey dots represent non-significant correlations with streamflow; significant negative correlations are blue ($p < 0.05$) and violet ($p < 0.01$) and significant positive correlations are orange ($p < 0.05$) and dark red ($p < 0.01$). (For interpretation of the references to colour in this figure legend, the reader is referred to the web version of this article.)

Table 2
Summary of associations between various atmospheric processes and instrumental streamflow by season in catchments used in Fig. 7. P and N indicate at least 50% of river catchments had a significant ($p < 0.5$ or $p < 0.01$) positive or negative correlation with the index. Grey indicates that between one third and half of the catchments were significantly correlated with the index. Where closer to one third were significantly correlated, most of those correlated river flows were significant at $p < 0.01$.

Region	STR_L	STR_I	SAM	Blocking	SOI/N34	DMI/DMI_E
JA						
Tasmania	P	N	N	N	P/N	
South Australian mainland	P	N	N		P/N	N/P
Central coast	N		P			
DJF						
Tasmania	P	N	N			
South Australian mainland						
Central coast	N	P	P		P/N	

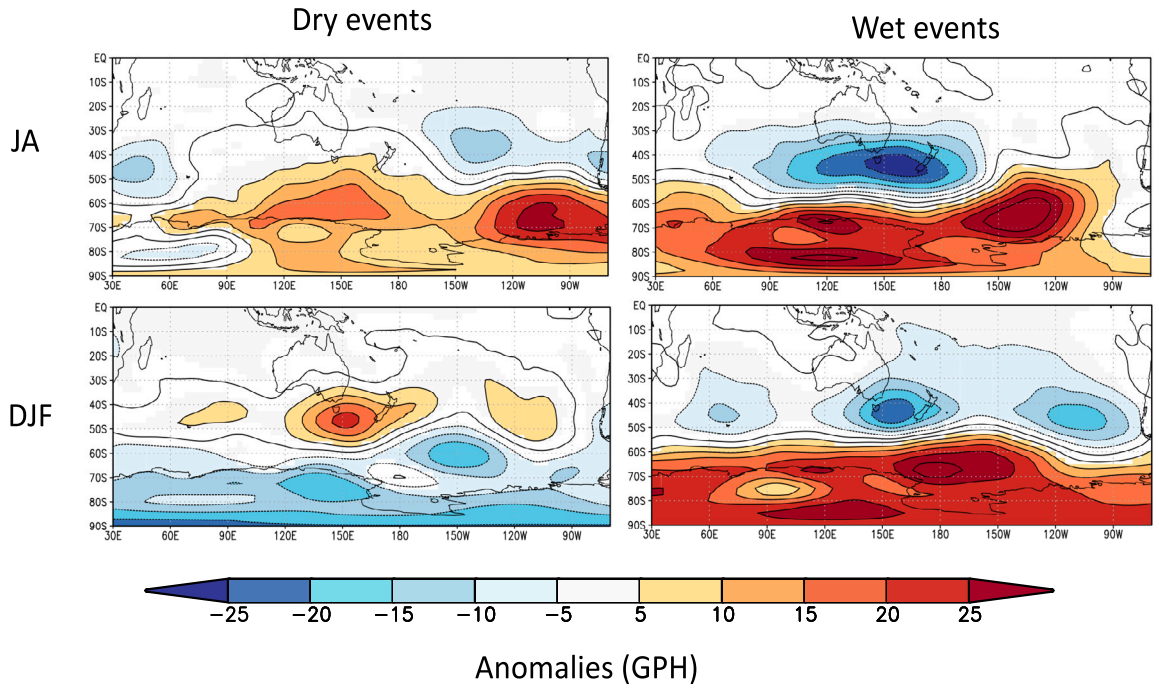

Fig. 6. Composites of the 850 GPH anomalies of 10 wettest (driest) events for the cool and warm season reconstructions compared to mean NCEP_NCAR (1948–2020) 850 mb height (two sided t-test, $p < 0.1$). Coloured regions represent significant anomalies. Equivalent plots but for instrumental data in Figure S3. (For interpretation of the references to colour in this figure legend, the reader is referred to the web version of this article.)

3.4. Implications for the use of remote proxies/reconstructions to infer hydroclimate

Our results show that the geographic relevance, or sign of relationship of reconstructions (e.g., our Tasmanian tree-ring based reconstructions) to, or with, a remote region (e.g., the southeastern Australian mainland) may vary by season. In our case, we surmise that the differences between the warm and cool seasonal applicability of our reconstructions are related to broadscale processes that drive hydroclimate and that themselves have distinct geographic and seasonal signatures (Table 2; Risbey et al., 2009; Verdon-Kidd and Kiem, 2009; Timbal and Drosdowsky, 2013). This creates challenges if seasonally defined reconstructions, or reconstructions based heavily on proxies with a strongly defined seasonal response, are used to make inferences for hydroclimate of other seasons in regions remote to the source area of proxies. This is particularly relevant for Australia where there is a lack of long-term *in situ* hydroclimate records for much of the continent, but where there is an urgent need for long-term information that hydroclimate proxies can provide. Some reconstructions try to account for this issue by utilising a two-tiered approach of screening for suitable proxies (Freund et al., 2017; Verdon-Kidd et al., 2017; Higgins et al., 2023). They do this by first identifying key hydroclimate drivers (e.g., ENSO) for the target region of interest and the other regions where these drivers are also known to have significant climate impacts. Proxies, or other records from these remote regions, that help produce robust reconstructions for the target region through a calibration/validation process such as described here, are then included as predictors.

Specifically, our results suggest that the west Tasmanian DJF flow reconstruction should not be used to represent summer hydroclimate across the southern Australian mainland, although we suggest (with caution) that it may provide ancillary information for the central east coast, but should not be used in isolation from *in situ* evidence (Fig. 7). On the other hand, the JA reconstruction may provide useful information about cool season hydroclimate variability across the far southeast of mainland Australia, an area that includes some of the City of Melbourne's water catchments.

Further, the seasonally specific reconstructions developed in this study are poorly related with three other flow reconstructions for southeastern Australia (Gallant and Gergis, 2011; Ho et al., 2015; Higgins et al., 2023) (Fig. 8) that target annual flow (Gallant et al.: Sep–Aug; Higgins et al.: June–May or Tozer et al.: Oct–Sep). It is, however, relevant to note some general similarities: declining flows in the Tozer et al. reconstruction and early 19th peak in the Gallant et al. reconstruction. There are also periods of similar trends between the DJF reconstruction and the Higgins et al. reconstruction in the 19th Century (Fig. 8). Overall, however, attempts to use seasonally defined reconstructions or proxies that respond predominantly to one season to represent *annual* hydroclimate should be approached with caution and rigorously verified.

Our case study highlights that attempts to compile information from hydroclimate reconstructions for Australia need to explicitly acknowledge regional and seasonal signatures, and avoid making inferences across too broad a spatial scale where this is inappropriate. This requires a strong appreciation of the nature of both the hydroclimatic drivers and their teleconnections, as well as the archives and proxies being utilised. While the modest strength of our reconstructions is an important caveat in our conclusion here, results in Table 2 and Figs. 5 and 7 indicate consistency with our understanding of the impacts of well-known climate drivers.

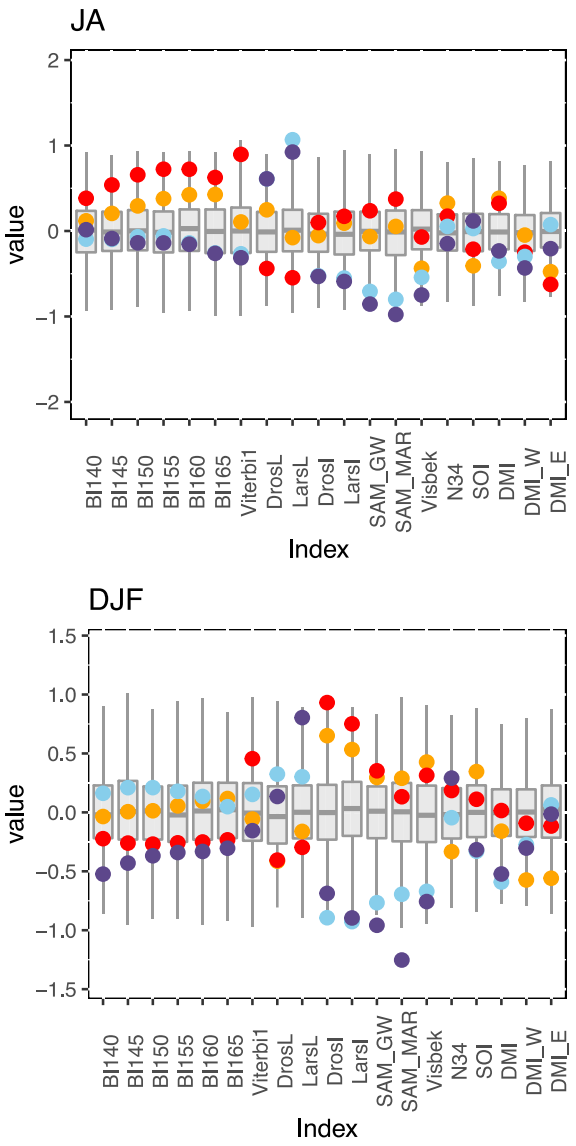

Fig. 7. Comparison of the means of the highest (lowest) flow composites for each season (dots) against the corresponding distribution (box plots) of means of 1000 samples of length of 10 years. Resampling from the 1940–2007 data was done with replacement. Orange (reconstruction) and red (instrumental) dots represent mean values of the indices for the 10 driest events. Blue (reconstruction) and purple (instrumental) represent the mean value of the respective index for the 10 wettest events. Dots beyond the upper and lower quartiles for an index indicate that the composite mean is moderately unusual. Dots at the extremity of the distribution suggest that the mean composite value is very unusual for that index (and hence suggest a relationship). Note that latitude of the STR uses negative degrees for the SH, and that *y*-axis scales differ for the two seasonal plots. (For interpretation of the references to colour in this figure legend, the reader is referred to the web version of this article.)

4. Conclusions

In this study we have presented the longest seasonally resolved streamflow reconstructions for far southeastern Australia. The ability to distinguish seasonal and geographic factors in long-term hydroclimate data for Australia will make a valuable contribution to understanding past Australian hydroclimate variability. The reconstructions indicate that longer and more intense wet and dry periods have occurred in the past during the warm season (e.g at the end of the 15th to start of the 16th Century for DJF). The long period of declining JA flow since the mid-20th Century is unusual in the context of the 450-year reconstruction, but consistent with other work. The general tendency towards increasing cumulative flow deficits when summer and winter are considered together is also unusual, although not unprecedented (e.g. mid 17th Century). Large cumulative deficits in western Tasmania may have significant implications for water-sensitive flora and dependent fauna that evolved under previous climate regimes. This needs to be considered by land and water managers in their planning. Continuing declines in inflows, especially if both DJF and JA are

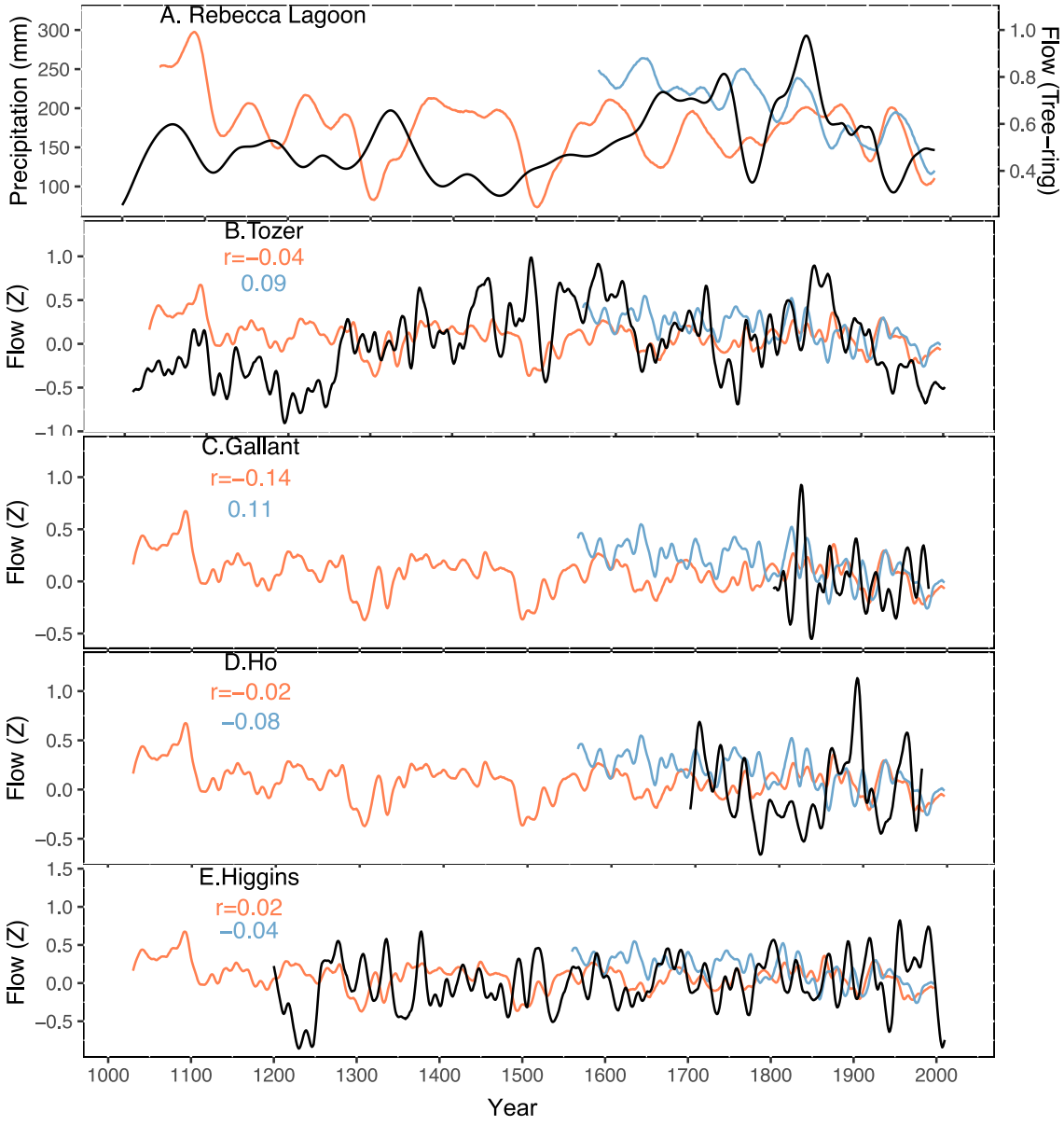

Fig. 8. Visual comparisons of the two new smoothed reconstructions with other hydroclimate reconstructions for southeastern Australia. A. Rebecca Lagoon precipitation reconstruction (Saunders et al., 2012). The published Rebecca lagoon reconstruction was smoothed using a 51-year filter (Saunders et al., 2012). For comparison purposes, the tree-ring reconstructions have also been smoothed with 51-year Gaussian smooth and a small linear adjustment made to allow better visual comparison with the Rebecca Lagoon record. B–E streamflow, all data smoothed with a 20-year Gaussian smooth; B. Williams River reconstruction (Tozer et al., 2018a); C. Murray River (Gallant and Gergis, 2011); D. (Ho et al., 2015) Murray River reconstruction; E. Murray River reconstruction 2 (Higgins et al., 2023) Correlations between the two reconstructions and annually resolved flow reconstructions also shown (these are for unsmoothed data). Orange colour is DJF, blue is JA. Black lines are the comparison reconstructions. (For interpretation of the references to colour in this figure legend, the reader is referred to the web version of this article.)

affected, will also have important implications for the ability to produce and export renewable hydro-power from these catchments. At the same time, evidence that droughts and pluvials longer than observed in the instrumental record have occurred under natural conditions effectively increases uncertainty around the possible impacts of anthropogenic climate change on hydroclimate in western Tasmania.

Our results point to the need to appreciate the diversity of regional hydroclimates. We highlight the key roles of STR (latitude and intensity) and SAM in driving west Tasmanian streamflow, and the seasonal differences in how Tasmanian streamflow is related to hydroclimate across southeastern Australia. These seasonal differences have important implications for water managers and others

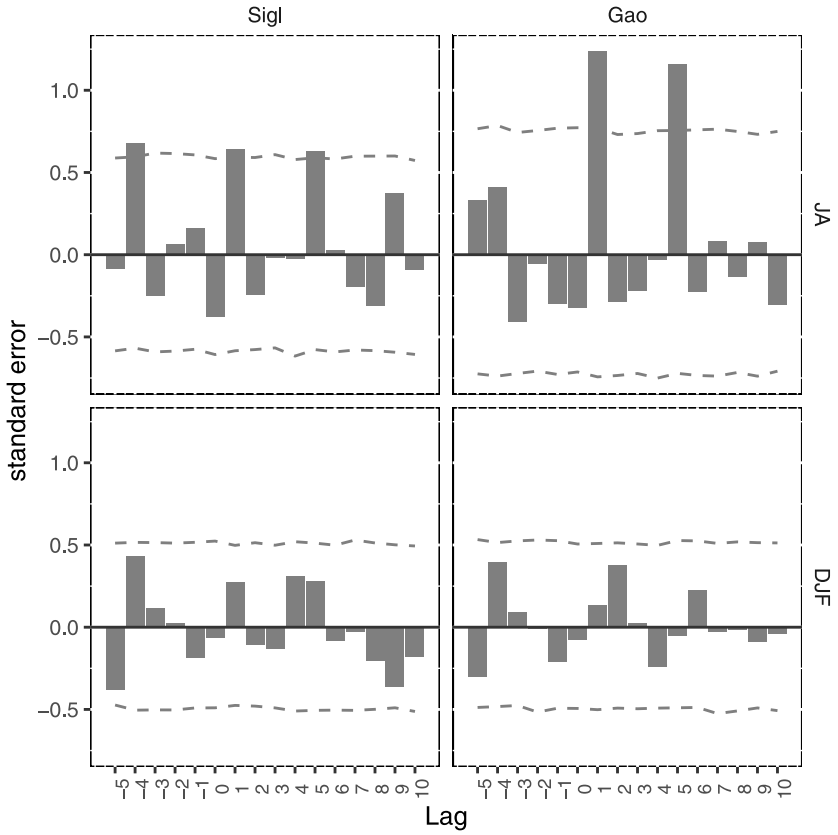

Fig. 9. Superposed epoch analysis using both the Gao et al. (2008) and Toohey and Sigl (2017) data. Dashed lines represent the 95% confidence interval based on 5000 iterations.

who seek to incorporate information from palaeo-reconstructions in their planning, particularly if those reconstructions are based on remote proxies that are also seasonally specific. Extrapolating seasonally based information to an annual scale may lead to flawed decision making, which is highly relevant if water resources are managed on a seasonal basis. These issues will be particularly acute for Australia where there are relatively few annually resolved reconstructions based on *in situ* information available. Therefore, there is a need to ensure available palaeo information is appropriately used to interpret Australia's high-resolution hydroclimatic past and to inform vital planning decisions for the future.

CRediT authorship contribution statement

Kathryn J. Allen: Conceptualization, Data curation, Formal analysis, Funding acquisition, Investigation, Methodology, Project administration, Resources, Software, Supervision, Validation, Visualization, Writing – original draft, Writing – review & editing. **Danielle C. Verdon-Kidd:** Conceptualization, Investigation, Methodology, Visualization, Writing – original draft, Writing – review & editing. **Mandy B. Freund:** Methodology, Visualization, Writing – original draft, Writing – review & editing. **Carly R. Tozer:** Methodology, Writing – original draft, Writing – review & editing. **Jonathan G. Palmer:** Conceptualization, Methodology, Writing – original draft, Writing – review & editing. **Philippa A. Higgins:** Methodology, Writing – original draft, Writing – review & editing. **Krystyna M. Saunders:** Data curation, Methodology, Writing – original draft, Writing – review & editing. **Patrick J. Baker:** Conceptualization, Funding acquisition, Project administration, Writing – original draft, Writing – review & editing.

Declaration of competing interest

The authors declare the following financial interests/personal relationships which may be considered as potential competing interests: Kathryn Allen reports financial support was provided by Australian Research Council.

Data availability

The data to produce the chronologies used to produce the reconstructions in this study are available on the NOAA palaeoclimatology site. Dam inflow data can be requested from Hydro Tasmania.

Acknowledgements

We would like to thank the many people who have assisted with fieldwork and provided technical assistance to develop the chronologies used in this work. Those who have provided substantial contributions include Scott Nichols, Holly Faulstich, Stella Thomas and Ken Felton. Carolyn Maxwell, Greg Carson, Fiona Ling, Stuart Allie and Mark Willis from Hydro Tasmania provided and assisted with interpretation of inflow records. The wood used to develop the chronologies utilised in the reconstructions shown here was collected with permits and permissions from Parks Tasmania, Forestry Tasmania, and Hydro Tasmania. We also thank Wasyl Drosdowsy (STR indices), Stuart Larsen (STR indices), Mike Pook (BI indices), Didier Monselesan (Viterbi index), and Martin Visbek (Visbek index) for having previously made their climate indices available. The collection, analysis, and interpretation of the tree-ring records has been supported by the Australian Research Council through grants LP12020081 and FT200100102.

Appendix A. Supplementary data

Supplementary material related to this article can be found online at https://doi.org/10.1016/j.ejrh.2024.101736.

References

Allen, K., Cook, E., Evans, R., Francey, R., Buckley, B., Palmer, J., Peterson, M., Baker, P., 2018. Lack of cool, not warm, extremes distinguishes late 20th century climate in 979-year Tasmanian summer temperature reconstruction. Environ. Res. Lett. 13 (3), 034041.

Allen, K., Freund, M., Palmer, J., Simkin, R., Williams, L., Brookhouse, M., Cook, E., Stewart, S., Baker, P., 2020a. Hydroclimate extremes in a north Australian drought reconstruction asymmetrically linked with central Pacific sea surface temperatures. Glob. Planet. Change 195, 103329.

Allen, K., Hope, P., Lam, D., Brown, J., Wasson, R., 2020b. Improving Australia's flood record for planning purposes–can we do better? Aust. J. Water Resour. 24 (1), 36–45.

Allen, K., Nichols, S., Evans, R., Allie, S., Carson, G., Ling, F., Cook, E., Lee, G., Baker, P., 2017. A 277 year cool season dam inflow reconstruction for Tasmania, southeastern Australia. Water Resour. Res. 53 (1), 400–414.

Allen, K., Nichols, S., Evans, R., Baker, P., 2022. Characteristics of a multi-species conifer network of wood properties chronologies from southern Australia. Dendrochronologia 76, 125997.

Allen, K., Nichols, S., Evans, R., Cook, E., Allie, S., Carson, G., Ling, F., Baker, P., 2015. Preliminary December–January inflow and streamflow reconstructions from tree rings for western Tasmania, southeastern Australia. Water Resour. Res. 51 (7), 5487–5503.

Björklund, J., Seftigen, K., Stoffel, M., Fonti, M.V., Kottlow, S., Frank, D.C., Esper, J., Fonti, P., Goosse, H., Grudd, H., et al., 2023. Fennoscandian tree-ring anatomy shows a warmer modern than medieval climate. Nature 620 (7972), 97–103.

Blake, S.A., Palmer, J.G., Björklund, J., Harper, J.B., Turney, C.S., 2020. Palaeoclimate potential of New Zealand Manoao colensoi (silver pine) tree rings using blue-intensity (BI). Dendrochronologia 60, 125664.

Brodribb, T.J., Cochard, H., 2009. Hydraulic failure defines the recovery and point of death in water-stressed conifers. Plant Physiol. 149 (1), 575–584.

Bunn, A.G., 2008. A dendrochronology program library in R (dplR). Dendrochronologia 26 (2), 115–124. http://dx.doi.org/10.1016/j.dendro.2008.01.002, URL: https://www.sciencedirect.com/science/article/pii/S1125786508000350.

Büntgen, U., Crivellaro, A., Arseneault, D., Baillie, M., Barclay, D., Bernabei, M., Bontadi, J., Boswijk, G., Brown, D., Christie, D.A., et al., 2022. Global wood anatomical perspective on the onset of the late antique little ice age (LALIA) in the mid-6th century CE. Sci. Bull. 67 (22), 2336–2344.

Burke, A., Innes, H.M., Crick, L., Anchukaitis, K.J., Byrne, M.P., Hutchison, W., McConnell, J.R., Moore, K.A., Rae, J.W., Sigl, M., et al., 2023. High sensitivity of summer temperatures to stratospheric sulfur loading from volcanoes in the northern hemisphere. Proc. Natl. Acad. Sci. 120 (47), e2221810120.

Cai, W., Cowan, T., Thatcher, M., 2012. Rainfall reductions over southern hemisphere semi-arid regions: the role of subtropical dry zone expansion. Sci. Rep. 2 (1), 702.

Cai, W., Sullivan, A., Cowan, T., 2011. Interactions of ENSO, the IOD, and the SAM in CMIP3 models. J. Clim. 24 (6), 1688–1704.

Chamberlayne, B.K., Tyler, J.J., Haynes, D., Shao, Y., Tibby, J., Gillanders, B.M., 2023. Hydrological change in southern Australia over 1750 years: a bivalve oxygen isotope record from the Coorong Lagoon. Clim. Past 19 (7), 1383–1396.

Chiew, F., Potter, N., Vaze, J., Petheram, C., Zhang, L., Teng, J., Post, D., 2014. Observed hydrologic non-stationarity in far south-eastern Australia: implications for modelling and prediction. Stoch. Environ. Res. Risk Assess. 28, 3–15.

Cole-Dai, J., 2010. Volcanoes and climate. Wiley Interdiscip. Rev. Clim. Change 1 (6), 824–839.

Consortium, P., et al., 2017. Comparing proxy and model estimates of hydroclimate variability and change over the common era. Clim. Past 13 (12), 1851–1900.

Cook, E.R., Meko, D.M., Stahle, D.W., Cleaveland, M.K., 1999. Drought reconstructions for the continental United States. J. Clim. 12 (4), 1145–1162.

Cook, E.R., Palmer, J.G., Ahmed, M., Woodhouse, C.A., Fenwick, P., Zafar, M.U., Wahab, M., Khan, N., 2013. Five centuries of upper indus river flow from tree rings. J. Hydrol. 486, 365–375.

Cook, B.I., Smerdon, J.E., Cook, E.R., Williams, A.P., Anchukaitis, K.J., Mankin, J.S., Allen, K., Andreu-Hayles, L., Ault, T.R., Belmecheri, S., et al., 2022. Megadroughts in the common era and the anthropocene. Nature Rev. Earth Environ. 3 (11), 741–757.

Dätwyler, C., Neukom, R., Abram, N.J., Gallant, A.J., Grosjean, M., Jacques-Coper, M., Karoly, D.J., Villalba, R., 2018. Teleconnection stationarity, variability and trends of the southern annular mode (SAM) during the last millennium. Clim. Dyn. 51 (5–6), 2321–2339.

Drew, D.M., Allen, K., Downes, G.M., Evans, R., Battaglia, M., Baker, P., 2013. Wood properties in a long-lived conifer reveal strong climate signals where ring-width series do not. Tree Physiol. 33 (1), 37–47.

Drosdowsky, W., 2005. The latitude of the subtropical ridge over eastern Australia: The l index revisited. Int. J. Climatol.: J. R. Meteorol. Soc. 25 (10), 1291–1299.

Evans, K., 2012. 'Antipodean England'? A History of Drought, Fire and Flood in Tasmania from European Settlement in 1803 to the 1960s (Ph.D. thesis). University of Tasmania.

Falster, G.M., Wright, N.M., Abram, N.J., Ukkola, A.M., Henley, B.J., 2023. Emerging anthropogenic influence on Australian multi-year droughts with potential for historically unprecedented megadroughts. EGUsphere 2023, 1–32.

Fletcher, M.-S., Benson, A., Bowman, D.M., Gadd, P.S., Heijnis, H., Mariani, M., Saunders, K.M., Wolfe, B.B., Zawadzki, A., 2018. Centennial-scale trends in the southern annular mode revealed by hemisphere-wide fire and hydroclimatic trends over the past 2400 years. Geology 46 (4), 363–366.

Fogt, R.L., Marshall, G.J., 2020. The southern annular mode: variability, trends, and climate impacts across the southern hemisphere. Wiley Interdiscip. Rev. Clim. Change 11 (4), e652.

Freund, M., Henley, B.J., Karoly, D.J., Allen, K.J., Baker, P.J., 2017. Multi-century cool-and warm-season rainfall reconstructions for Australia's major climatic regions. Clim. Past 13 (12), 1751–1770.

Friedman, J.H., 1984. Smart User's Guide. Laboratory for Computational Statistics, Stanford University Stanford.

Gallant, A.J., Gergis, J., 2011. An experimental streamflow reconstruction for the River Murray, Australia, 1783–1988. Water Resour. Res. 47 (12).

Gao, C., Robock, A., Ammann, C., 2008. Volcanic forcing of climate over the past 1500 years: An improved ice core-based index for climate models. J. Geophys. Res.: Atmos. 113 (D23).
Grose, M., Barnes-Keoghan, I., Corney, S., White, C., Holz, G., Bennett, J., Gaynor, S., Bindoff, N., 2010. Climate futures for Tasmania: general climate impacts technical report. antarctic climate & ecosystems cooperative research centre, Hobart, Tasmania. Clim. Futures Tasmania 3.
Heinrich, I., Weidner, K., Helle, G., Vos, H., Banks, J.C., 2008. Hydroclimatic variation in far north queensland since 1860 inferred from tree rings. Palaeogeogr. Palaeoclimatol. Palaeoecol. 270 (1–2), 116–127.
Heinrich, I., Weidner, K., Helle, G., Vos, H., Lindesay, J., Banks, J.C., 2009. Interdecadal modulation of the relationship between ENSO, IPO and precipitation: insights from tree rings in Australia. Clim. Dyn. 33, 63–73.
Hendon, H.H., Lim, E.-P., Nguyen, H., 2014. Seasonal variations of subtropical precipitation associated with the southern annular mode. J. Clim. 27 (9), 3446–3460.
Higgins, P., Palmer, J., Andersen, M., Turney, C., Johnson, F., Allen, K., Verdon-Kidd, D., Cook, E., 2023. Examining past and projecting future: an 800-year streamflow reconstruction of the Australian murray river. Environ. Res. Lett. 18 (10), 104016.
Higgins, P.A., Palmer, J.G., Turney, C.S., Andersen, M.S., Johnson, F., 2022. Do southern hemisphere tree rings record past volcanic events? A case study from New Zealand. Clim. Past 18 (5), 1169–1188.
Hill, K.J., Santoso, A., England, M.H., 2009. Interannual Tasmanian rainfall variability associated with large-scale climate modes. J. Clim. 22 (16), 4383–4397. http://dx.doi.org/10.1175/2009JCLI2769.1, URL: https://journals.ametsoc.org/view/journals/clim/22/16/2009jcli2769.1.xml.
Ho, M., Kiem, A.S., Verdon-Kidd, D.C., 2015. A paleoclimate rainfall reconstruction in the murray-darling basin (MDB), Australia: 2. Assessing hydroclimatic risk using paleoclimate records of wet and dry epochs. Water Resour. Res. 51 (10), 8380–8396.
Holgate, C., Evans, J.P., Taschetto, A.S., Gupta, A.S., Santoso, A., 2022. The impact of interacting climate modes on east Australian precipitation moisture sources. J. Clim. 35 (10), 3147–3159.
Jones, D.A., Wang, W., Fawcett, R., 2009. High-quality spatial climate data-sets for Australia. Aust. Meteorol. Oceanogr. J. 58 (4), 233.
Kiem, A.S., Vance, T.R., Tozer, C.R., Roberts, J.L., Dalla Pozza, R., Vitkovsky, J., Smolders, K., Curran, M.A., 2020. Learning from the past–using palaeoclimate data to better understand and manage drought in South East Queensland (SEQ), Australia. J. Hydrol.: Reg. Stud. 29, 100686.
King, J., Anchukaitis, K.J., Allen, K., Vance, T., Hessl, A., 2023. Trends and variability in the southern annular mode over the common era. Nature Commun. 14 (1), 2324.
King, A.D., Klingaman, N.P., Alexander, L.V., Donat, M.G., Jourdain, N.C., Maher, P., 2014. Extreme rainfall variability in Australia: patterns, drivers, and predictability. J. Clim. 27 (15), 6035–6050.
Larsen, S.H., Nicholls, N., 2009. Southern Australian rainfall and the subtropical ridge: Variations, interrelationships, and trends. Geophys. Res. Lett. 36 (8).
Ljungqvist, F.C., Piermattei, A., Seim, A., Krusic, P.J., Büntgen, U., He, M., Kirdyanov, A.V., Luterbacher, J., Schneider, L., Seftigen, K., et al., 2020. Ranking of tree-ring based hydroclimate reconstructions of the past millennium. Quat. Sci. Rev. 230, 106074.
Lough, J.M., 2007. Tropical river flow and rainfall reconstructions from coral luminescence: Great Barrier Reef, Australia. Paleoceanography 22 (2).
Lough, J.M., 2011. Great Barrier Reef coral luminescence reveals rainfall variability over northeastern Australia since the 17th century. Paleoceanography 26 (2).
Lough, J., Lewis, S., Cantin, N., 2015. Freshwater impacts in the central Great Barrier Reef: 1648–2011. Coral Reefs 34, 739–751.
Ma, Y., Sun, J., Dong, T., Yu, W., Dong, W., 2022. More profound impact of CP ENSO on Australian spring rainfall in recent decades. Clim. Dynam. 1–15.
Maher, P., Sherwood, S.C., 2014. Disentangling the multiple sources of large-scale variability in Australian wintertime precipitation. J. Clim. 27 (17), 6377–6392.
Martin-Benito, D., Beeckman, H., Canellas, I., 2013. Influence of drought on tree rings and tracheid features of Pinus nigra and Pinus sylvestris in a mesic Mediterranean forest. Eur. J. Forest Res. 132, 33–45.
Masson-Delmotte, V., Zhai, P., Pirani, S., Connors, C., Péan, S., Berger, N., Caud, Y., Chen, L., Goldfarb, M., Scheel Monteiro, P.M., 2021. IPCC, 2021: Summary for policymakers. In: Climate Change 2021: The Physical Science Basis. Contribution of Working Group I to the Sixth Assessment Report of the Intergovernmental Panel on Climate Change. Cambridge University Press, Cambridge, United Kingdom and New York, NY, USA.
McBride, J.L., Nicholls, N., 1983. Seasonal relationships between Australian rainfall and the southern oscillation. Mon. Weather Rev. 111 (10), 1998–2004.
Melvin, T.M., Briffa, K.R., 2008. A "signal-free" approach to dendroclimatic standardisation. Dendrochronologia 26 (2), 71–86.
Melvin, T.M., Briffa, K.R., Nicolussi, K., Grabner, M., 2007. Time-varying-response smoothing. Dendrochronologia 25 (1), 65–69.
Murphy, B.F., Timbal, B., 2008. A review of recent climate variability and climate change in southeastern Australia. Int. J. Climatol.: J. R. Meteorol. Soc. 28 (7), 859–879.
Nguyen, H., Lucas, C., Evans, A., Timbal, B., Hanson, L., 2015. Expansion of the southern hemisphere hadley cell in response to greenhouse gas forcing. J. Clim. 28 (20), 8067–8077.
Nicholls, N., Gruza, G., Jouzel, J., Karl, T., Ogallo, L., Parker, D., et al., 1996. Observed Climate Variability and Change. Cambridge University Press Cambridge.
O'Donnell, A.J., McCaw, W.L., Cook, E.R., Grierson, P.F., 2021. Megadroughts and pluvials in southwest Australia: 1350–2017 CE. Clim. Dynam. 57, 1817–1831.
Palmer, J.G., Cook, E.R., Turney, C.S., Allen, K., Fenwick, P., Cook, B.I., O'Donnell, A., Lough, J., Grierson, P., Baker, P., 2015. Drought variability in the eastern Australia and New Zealand summer drought atlas (ANZDA, CE 1500–2012) modulated by the interdecadal Pacific oscillation. Environ. Res. Lett. 10 (12), 124002.
Peel, M.C., McMahon, T.A., Finlayson, B.L., 2004. Continental differences in the variability of annual runoff-update and reassessment. J. Hydrol. 295 (1–4), 185–197.
Pezza, A.B., Durrant, T., Simmonds, I., Smith, I., 2008. Southern hemisphere synoptic behavior in extreme phases of SAM, ENSO, sea ice extent, and southern Australia rainfall. J. Clim. 21 (21), 5566–5584.
Pook, M., Risbey, J., McIntosh, P., Ummenhofer, C., Marshall, A., Meyers, G., 2013. The seasonal cycle of blocking and associated physical mechanisms in the Australian region and relationship with rainfall. Mon. Weather Rev. 141 (12), 4534–4553.
Post, D.A., Timbal, B., Chiew, F.H., Hendon, H.H., Nguyen, H., Moran, R., 2014. Decrease in southeastern Australian water availability linked to ongoing Hadley cell expansion. Earth's Future 2 (4), 231–238.
Power, S., Casey, T., Folland, C., Colman, A., Mehta, V., 1999. Inter-decadal modulation of the impact of ENSO on Australia. Clim. Dyn. 15, 319–324.
Risbey, J.S., Pook, M.J., McIntosh, P.C., Wheeler, M.C., Hendon, H.H., 2009. On the remote drivers of rainfall variability in Australia. Mon. Weather Rev. 137 (10), 3233–3253.
Rocha, E., Gunnarson, B.E., Holzkämper, S., 2020. Reconstructing summer precipitation with MXD data from Pinus sylvestris growing in the Stockholm Archipelago. Atmosphere 11 (8), 790.
Saunders, K., Kamenik, C., Hodgson, D.A., Hunziker, S., Siffert, L., Fischer, D., Fujak, M., Gibson, J.A., Grosjean, M., 2012. Late holocene changes in precipitation in northwest Tasmania and their potential links to shifts in the southern hemisphere westerly winds. Glob. Planet. Change 92, 82–91.
Schneider, L., Smerdon, J.E., Büntgen, U., Wilson, R.J., Myglan, V.S., Kirdyanov, A.V., Esper, J., 2015. Revising midlatitude summer temperatures back to AD 600 based on a wood density network. Geophys. Res. Lett. 42 (11), 4556–4562.
Seftigen, K., Goosse, H., Klein, F., Chen, D., 2017. Hydroclimate variability in Scandinavia over the last millennium–insights from a climate model–proxy data comparison. Clim. Past 13 (12), 1831–1850.
Stockton, C.W., Jacoby, G., 1976. Long-term surface-water supply and streamflow trends in the upper colorado river basin. Available from the National Technical Information Service, Springfield VA 22161 as PB-264 533, Price codes: A 05 in paper copy, A 01 in microfiche. Lake Powell Research Project Bulletin 18.

Timbal, B., Drosdowsky, W., 2013. The relationship between the decline of southeastern Australian rainfall and the strengthening of the subtropical ridge. Int. J. Climatol. 33 (4), 1021–1034.
Toohey, M., Sigl, M., 2017. Volcanic stratospheric sulfur injections and aerosol optical depth from 500 BCE to 1900 CE. Earth Syst. Sci. Data 9 (2), 809–831.
Tozer, C., Kiem, A., Vance, T., Roberts, J., Curran, M., Moy, A., 2018a. Reconstructing pre-instrumental streamflow in eastern Australia using a water balance approach. J. Hydrol. 558, 632–646.
Tozer, C.R., Risbey, J.S., O'Kane, T.J., Monselesan, D.P., Pook, M.J., 2018b. The relationship between wave trains in the southern hemisphere storm track and rainfall extremes over Tasmania. Mon. Weather Rev. 146 (12), 4201–4230.
Tozer, C.R., Vance, T.R., Roberts, J.L., Kiem, A.S., Curran, M.A., Moy, A.D., 2016. An ice core derived 1013-year catchment-scale annual rainfall reconstruction in subtropical eastern Australia. Hydrol. Earth Syst. Sci. 20 (5), 1703–1717.
Van Dijk, A.I., Beck, H.E., Crosbie, R.S., De Jeu, R.A., Liu, Y.Y., Podger, G.M., Timbal, B., Viney, N.R., 2013. The millennium drought in southeast Australia (2001–2009): Natural and human causes and implications for water resources, ecosystems, economy, and society. Water Resour. Res. 49 (2), 1040–1057.
Vance, T.R., Kiem, A.S., Jong, L.M., Roberts, J.L., Plummer, C.T., Moy, A.D., Curran, M.A., van Ommen, T.D., 2022. Pacific decadal variability over the last 2000 years and implications for climatic risk. Commun. Earth Environ. 3 (1), 33.
Vance, T., Roberts, J., Plummer, C., Kiem, A., Van Ommen, T., 2015. Interdecadal Pacific variability and eastern Australian megadroughts over the last millennium. Geophys. Res. Lett. 42 (1), 129–137.
Verdon-Kidd, D.C., Hancock, G.R., Lowry, J.B., 2017. A 507-year rainfall and runoff reconstruction for the Monsoonal north west, Australia derived from remote paleoclimate archives. Glob. Planet. Change 158, 21–35.
Verdon-Kidd, D.C., Kiem, A.S., 2009. Nature and causes of protracted droughts in southeast Australia: Comparison between the federation, WWII, and big dry droughts. Geophys. Res. Lett. 36 (22).
Verdon-Kidd, D.C., Kiem, A.S., 2010. Quantifying drought risk in a nonstationary climate. J. Hydrometeorol. 11 (4), 1019–1031.
Vinod, H.D., López-de Lacalle, J., 2009. Maximum entropy bootstrap for time series: the meboot R package. J. Stat. Softw. 29, 1–19.
Williams, A.A., Stone, R.C., 2009. An assessment of relationships between the Australian subtropical ridge, rainfall variability, and high-latitude circulation patterns. Int. J. Climatol.: J. R. Meteorol. Soc. 29 (5), 691–709.
Wilson, R., Allen, K., Baker, P., Boswijk, G., Buckley, B., Cook, E., D'Arrigo, R., Druckenbrod, D., Fowler, A., Grandjean, M., et al., 2021. Evaluating the dendroclimatological potential of blue intensity on multiple conifer species from Tasmania and New Zealand. Biogeosciences 18 (24), 6393–6421.
Woodhouse, C.A., Meko, D.M., MacDonald, G.M., Stahle, D.W., Cook, E.R., 2010. A 1,200-year perspective of 21st century drought in southwestern north America. Proc. Natl. Acad. Sci. 107 (50), 21283–21288.